

The high-pressure behavior of micas: Vibrational spectra of muscovite, biotite, and phlogopite to 30 GPa

QUENTIN WILLIAMS,^{1,*} ELISE KNITTLE,¹ HENRY P. SCOTT,² AND ZHENXIAN LIU³

¹Department of Earth and Planetary Sciences, University of California, Santa Cruz, California 95064, U.S.A.

²Department of Physics and Astronomy, Indiana University South Bend, South Bend, Indiana 46634, U.S.A.

³Geophysical Laboratory, Carnegie Institution of Washington, 5251 Broad Branch Road NW, Washington, D.C. 20015, U.S.A.

ABSTRACT

The infrared spectra of natural samples of muscovite, biotite, and phlogopite are characterized to pressures of ~30 GPa, as is the Raman spectrum of muscovite to ~8 GPa. Both far-infrared and mid-infrared data are collected for muscovite, and mid-infrared data for biotite and phlogopite. The response of the hydroxyl vibrations to compression differs markedly between the dioctahedral and trioctahedral micas: the hydrogen bonding in dioctahedral environments increases with pressure, as manifested by shifts to lower frequency of the hydroxyl-stretching vibrations, whereas cation-hydrogen repulsion likely produces shifts to higher frequency of the hydroxyl vibrations within trioctahedral environments. An abrupt decrease in frequency and increase in band width of the hydroxyl-stretching vibration in muscovite is observed at pressures above ~18–20 GPa, implying that the previously documented pressure-induced disordering is associated with the local environment and shifts in location of the hydroxyl unit in this material. The far-infrared vibrations of muscovite indicate that its compressional mechanism changes above 5–8 GPa, as the K-O stretching vibration with a zero-pressure frequency near 112 cm⁻¹ shifts in its pressure dependence from 6.9 cm⁻¹/GPa below this pressure range to 0.78 cm⁻¹/GPa above it. Thus, it appears that the magnitude of interlayer compression is decreased above this pressure, and hence that the compression of muscovite may become less strongly anisotropic. The mid-infrared bands that are primarily produced by vibrations of the tetrahedral layer broaden under pressure in both muscovite and biotite: within biotite, a spectral region that may be associated with higher coordination of tetrahedral cations increases in amplitude above about 25 GPa. The corresponding bands in phlogopite undergo less broadening, and their behavior is fully reversible on decompression.

Keywords: Muscovite, biotite, phlogopite, micas, pressure, amorphization, hydrogen bonding

INTRODUCTION

The high-pressure properties of micas are important because they concern: (1) the manner in which water is retained in the upper mantle of the planet (e.g., Domanik and Holloway 1996; Williams and Hemley 2001; Poli and Schmidt 2002; Williams 2007); (2) the genesis of magmas at depth within subduction zones (e.g., Sudo and Tatsumi 1990; Schmidt et al. 2004; Hirschmann 2006; Thomsen and Schmidt 2008); (3) the mechanism for alkali element retention in the upper mantle; and (4) the role they may play in subduction dynamics due to their anomalous rheology (Stockhert et al. 1999). Indeed, both the presence of micas within deeply derived xenoliths and experimental studies on the stabilities of micas within a range of assemblages demonstrate that micas are important hosts of water and alkali elements within the upper mantle of the planet. Phlogopitic and phengitic micas have been frequently observed in both kimberlites and as inclusions in exhumed peridotites (e.g., Downes et al. 2004; Reguir et al. 2009). Moreover, the behavior of hydrated layered phases under pressure has considerable interest for the high-pressure crystal chemistry of materials (e.g., Dera et al. 2003; Butler and Frost 2006; Scott et al. 2007).

Considerable effort has been devoted to characterizing the elastic response of micas to compression, particularly in the pressure range up to 6–10 GPa (Comodi and Zanazzi 1995; Pavese et al. 2003; Comodi et al. 2004; Gatta et al. 2010). At higher pressures, results are considerably sparser, but anomalous results have been observed at pressures in the 15 to 30 GPa range. Specifically, Curetti et al. (2006) have observed that the pressure dependence of both lattice parameter ratios and the *b* unit-cell parameter change dramatically above ~16 GPa in a natural 2M₁-phengite on the muscovite-celadonite join. Gatta et al. (2010) attributed this change in behavior to a decrease in crystallinity initiating in the 15–17 GPa range. Faust and Knittle (1994) observed that long-range crystalline order, as determined from the complete disappearance of the X-ray diffraction pattern, was lost in end-member muscovite at pressures above 27 GPa, with disordering appearing to commence near 18 GPa. Indeed, as micas have highly anisotropic low-pressure elastic properties, with their initial compressibility along the *c*-axis typically being 4–6 times greater than the compressibility within the layers (Gatta et al. 2010; Comodi and Zanazzi 1995), the higher-pressure effects and degree of persistence of this low-pressure compressional anisotropy remains unclear.

Although extensive X-ray characterizations of micas under pressure have been conducted, there are comparatively few high-

* E-mail: qwilliams@pmc.ucsc.edu

pressure spectroscopic measurements. As a single example, Holtz et al. (1993) examined limited portions of the Raman spectrum of biotite and muscovite to 1.5 and 2.5 GPa, respectively, but few other high-pressure spectroscopic characterizations of micas exist. This paucity is notable, as vibrational spectroscopy yields fundamental insights into the bonding of hydroxyl units and the response of the silicate layers to compression. Here, we present a suite of infrared spectra of $KAl_2Si_3AlO_{10}(OH)_2$ -muscovite, $KMg_3Si_3AlO_{10}(OH)_2$ -phlogopite, and $K(Mg,Fe)_3Si_3AlO_{10}(OH)_2$ -biotite to pressures of 30 GPa. Our results on muscovite span from the far-infrared to the hydroxyl-stretching vibrations, whereas our results on biotite and phlogopite encompass mid-infrared and hydroxyl vibrations. Our choice of these compositions is motivated not only by the geologic importance of these compositions, but also because they span both dioctahedral and trioctahedral structural types. Indeed, phlogopite has three octahedral cations coordinating the hydroxyl anion, muscovite has two octahedral cations and a vacancy, and biotite contains both trioctahedral and dioctahedral environments, with the vacancies associated with the dioctahedral configuration being induced by the presence of trivalent iron. Moreover, the microstructural origins of disordering and amorphization within muscovite remain enigmatic, and the possible occurrence of such behavior in other metastably compressed micas is ill-constrained. The vibrational spectroscopic data that we present are anticipated to be primarily sensitive to local structural environments within the crystals, and thus to the degree of local disorder. The onset of disordering may be precursory to amorphization (which is typically determined by means of diffraction techniques), and extensive disordering may ultimately generate amorphization. Thus, our data provide constraints on not only the differing high-pressure response of dioctahedral and trioctahedral structural environments within layered hydrous phases, but also on the microstructural origins of metastable high-pressure transitions in these materials.

EXPERIMENTAL METHODS

Natural samples of each of the three micas were utilized. The muscovite sample is from Methuen Township, Ontario, provided by the Harvard Museum, and is the same material as that characterized and used in shock experiments by Sekine et al. (1991) and by Faust and Knittle (1994) in their static compression study. It is a monoclinic polytype with space group $C2/c$ and $2M_1$ symmetry, and has a composition that is closely approximated by $K_{0.92}Na_{0.08}Al_3Si_3O_{10}(OH)_2$ (Sekine et al. 1991; Faust and Knittle 1994). The biotite is from Bancroft, Ontario, by way of Ward's Scientific Establishment, Inc., with $C2/m$ symmetry, and occurs as the $1M$ polytype. The composition of this material, as determined by electron microprobe, is similar to prior measurements of samples from this locality (Chon et al. 2003; Samson et al. 2005) and is approximately $(K_{1.89}Na_{0.11})(Mg_{5.22}Fe_{2.30}Ti_{0.30}Mn_{0.07})(Al_{1.94}Si_{5.95})O_{20}(OH,F)_4$. The phlogopite used is from the well-known North Burgess, Ontario locality. It has an approximate composition of $(K_{0.95}Na_{0.05}Ca_{0.01})(Mg_{2.78}Fe_{0.15}Al_{0.05}Ti_{0.01})(Al_{1.11}Si_{2.89})O_{10}(OH,F)_2$, $C2/m$ symmetry, and is from Ward's Scientific. Biotite and phlogopite samples were taken from the cores of ~ 10 cm diameter and ~ 1 cm thick books of these micas, and their identification was confirmed by conventional powder X-ray diffraction.

The mid-infrared spectra were collected using an evacuated IFS-66v Bruker Fourier transform infrared spectrometer (FTIR), equipped with, depending on spectral range, either a KBr or CaF₂ beamsplitter, globar source, and either a MCT or InSb detector. All mid-infrared spectra were collected with a spectral resolution of 4 cm⁻¹, and extend to a detector-modulated lower frequency limit of ~ 560 cm⁻¹. Because of the weakness of the hydroxyl vibrations in trioctahedral micas, separate runs with different concentrations of sample were sometimes required to collect data on both the hydroxyl-stretching and silicate-stretching vibrations. Either Merrill-Bassett or Mao-Bell type diamond cells were used to generate pressures. Samples were compressed in spring-steel gaskets using KBr as the pressure medium, with

approximately 10 wt% sample for the mid-infrared experiments between 500 and 1300 cm⁻¹, and ~ 35 wt% sample for the measurements of the hydroxyl vibrations of biotite. This difference in concentration was due to the dramatically different absorption coefficients of the silicate and hydroxyl-stretching bands, and the effect of spectral fringing on the hydroxyl vibrations. In all experiments, pressure variations within the samples were monitored with multiple ruby grains within the sample and, at the peak pressures on compression, these variations did not exceed 10% of the total pressure; somewhat larger pressure gradients (up to 15%) were observed on decompression. Although these experiments are not hydrostatic, it is well known that no hydrostatic media exist above ~ 10 GPa at 300 K (Klotz et al. 2009). Moreover, in hydrated materials that do not undergo a phase transition, such experiments typically produce modestly broadened, but fully reversible (in terms of both shift and peak width) hydroxyl-stretching vibrations at the highest pressure conditions of the experiments; similarly, the width of silicate-associated bands may be modestly affected by non-hydrostaticity (Bradbury and Williams 2003; Scott et al. 2007). Characteristic particle sizes were ~ 5 μ m diameter platelets, with typical thicknesses of a couple of micrometers. The platy character of mica samples renders mid-infrared spectroscopy under pressure challenging: internal reflections within the mica sheets, if they are oriented normal to the infrared beam, can produce ubiquitous strong fringing across the spectra. Hence, considerable care was taken in the preparation of samples for mid-infrared measurements to manually randomize the orientation of the mica fragments within the salt matrix: even with these measures, fringing sometimes occurred within the spectra. The hydroxyl vibrations of biotite and phlogopite (which are weaker than those of muscovite) were particularly prone to difficulties associated with fringing: in the case of biotite, separate hydroxyl measurements were made. Far-infrared spectra were collected using the synchrotron source at beamline U2A of the National Synchrotron Light Source, using an IFS-66v Bruker spectrometer equipped with a liquid-He-cooled bolometer and a custom-made vacuum infrared microscope; the experimental configuration produced an upper frequency limit of 480 cm⁻¹ for the far-infrared spectra. Samples were prepared by pressing the mica into a thin film of roughly 5 μ m thickness, and mounting the mica within petroleum jelly into a 100 μ m diameter T301 stainless steel gasket hole. The petroleum jelly served as both the pressure medium and a far-infrared window. Optical fringing was a substantially less severe problem for the far-infrared spectra, due to the longer wavelengths of far-infrared light. The Raman spectra of muscovite were collected using samples loaded in a methanol:ethanol pressure medium, using an apparatus described elsewhere (Williams and Knittle 1996; Knittle et al. 2001). The resolution of these spectra is ~ 3 cm⁻¹.

RESULTS

Muscovite

Mid-infrared spectra of muscovite on compression and decompression are shown in Figures 1a and 1b, far-infrared spectra in Figure 1c, and mode shifts with pressure are plotted in Figure 2. The zero-pressure peak positions (Table 1) agree well with prior mid-infrared studies (e.g., Vedder 1964; Velde 1978). The assignments of mid-infrared bands in Table 1 are derived from a combination of the semi-empirical assignments given in Farmer (1974) and Langer et al. (1981) and the normal coordinate analysis of McKeown et al. (1999a). The assignments of most bands between different sources are quite similar: the one exception is that the bands with zero-pressure frequencies of 751 and 912 cm⁻¹ are not present in the calculated infrared spectrum of McKeown et al. (1999a). In the former case, a general consensus exists that this band is a T-O-T bending vibration, probably involving aluminum in the tetrahedral sites (Langer et al. 1981). In the latter case, Vedder and McDonald (1963) have clearly demonstrated using deuterated muscovite that this vibration is associated with a libration of the hydroxyl unit. As will be described below, the pressure shift of the 912 cm⁻¹ band is also notably lower than that of the silicate-associated bands (Figs. 1 and 2; Table 1): hydroxyl librations have been observed to typically have substantially lower pressure shifts than silicate-associated bands (e.g., Scott et al. 2007).

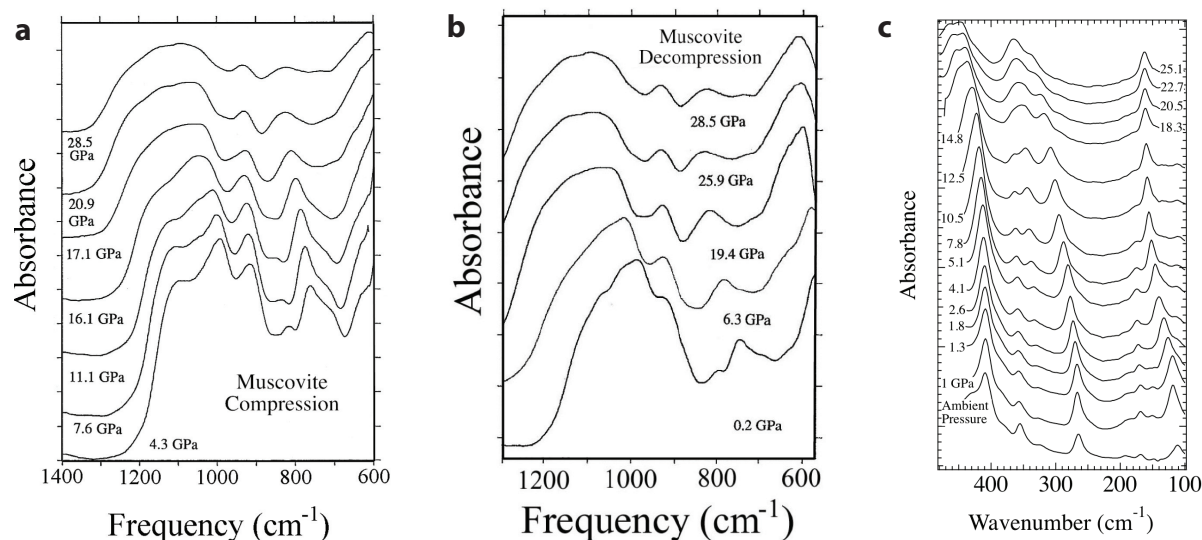


FIGURE 1. (a) Representative mid-infrared spectra of muscovite on compression at high pressures. Absorbance is in arbitrary units. (b) Representative mid-infrared spectra of muscovite on decompression. (c) Representative far-infrared spectra of muscovite on compression.

TABLE 1. Mode shifts, assignments, and Grüneisen parameters of the vibrational spectrum of muscovite

ν_0 (cm^{-1})	Pressure shift ($\text{cm}^{-1}/\text{GPa}$)	σ	Assignment	Mode γ	
3635	-0.06		O-H Stretch	-0.001	MIR
1070	4.13	0.34	T-O(apical) Stretch	0.23	MIR
988	2.30	0.74	T-O(basal) Stretch	0.14	MIR
912	1.15	0.09	O-H Libration	0.08	MIR
801	4.27	0.13	T-O-T Bend	0.32	MIR
751	3.05	0.08	T(Al)-O-T(Al) Bend	0.24	MIR
701	1.80	0.23	O out-of-plane Trans.+M-O Str.	0.15	Raman
409	0.75	0.12	O(br) out-of-plane Trans.	0.11	FIR
401	1.74	1.30	M2 Trans. + O Trans.	0.26	Raman
355	0.95	0.20	K in-plane Trans. + M2 Trans.	0.16	FIR
325	1.55	0.04	K-Trans., M2 Trans.	0.29	FIR
264	3.50	0.17	O(nb) Trans.	0.80	FIR
259	4.32	0.65	O Trans. + K Trans.	1.00	Raman
212	1.51	0.32	O,OH Trans. + K Trans.	0.43	Raman
168	1.54	0.19	OH-M2-OH bend	0.55	FIR
148	1.60	0.36	K-Trans. + O(nb) Trans.	0.65	FIR
112	6.90	0.39	K-translation	3.70	FIR
100*	0.86*	0.20	Sheet Trans.	0.52	Raman

Notes: MIR fits conducted on compressional data to 16 GPa, except for the 988 cm^{-1} band which was fit to 11 GPa. FIR fits to 5.1 GPa, except for the 325 cm^{-1} band, which was based on all data on this band; the hydroxyl-stretching vibration was fit to a quadratic.

* From Holtz et al. (1993).

The high-pressure mid-infrared results (Figs. 1 and 2) are characterized by a systematic, but variable, shift of all bands to higher frequency, with a progressive broadening and merging of the silicate stretching bands above 17 GPa. Mode shifts of the mid-infrared bands are calculated based on shifts to 16 GPa (with the exception of the 988 cm^{-1} band), as above this pressure bands undergo substantial broadening (Table 1). Nevertheless, the silicate stretching bands with initial frequencies of 988 and 1070 cm^{-1} appear to undergo shifts at pressures above 16 GPa that may exceed their lower pressure values (Figs. 1a and 2), with the 988 cm^{-1} band appearing to have an increased pressure shift above ~ 8 GPa. Thus, the magnitude of compaction of the tetrahedra in muscovite may be larger at higher pressures than at lower pressures, where interlayer compaction provides the dominant means of compression. Moreover, unlike the silica

polymorphs and feldspars, muscovite does not show a notable increase in absorption in the 600–800 cm^{-1} range when compressed in the 20–30 GPa range: such a shift in amplitude has been associated with an increase in coordination of silicon cations under metastable compression (Williams et al. 1993; Williams 1998). Hence, it appears that the local tetrahedral environment of the silicon cations persists to the highest pressures of these measurements. On decompression, the results are clearly not fully reversible (Fig. 1b). The broadening and loss of definition of the silicate stretching bands persists to pressures substantially below 10 GPa.

Far-infrared results on muscovite are shown in Figure 1c. The ambient-pressure spectrum is very similar to a range of previous measurements (Loh 1973; Tateyama et al. 1977; Velde and Couty 1985; Schroeder 1990; Diaz et al. 2000). In the far-infrared,

there are some inconsistencies in detailed mode assignments (e.g., McKeown et al. 1999a; Diaz et al. 2000), but most assign the band near 112 cm^{-1} to a K-O stretching vibration, probably residing in the *a-b* plane, the 148 cm^{-1} band to an out-of-plane displacement of the K-ion, the 168 cm^{-1} to displacements of O atoms associated with the octahedral layer and the 264 cm^{-1} band to a lattice vibration associated with displacements of non-bridging oxygen ions (Loh 1973; Schroeder 1990; Diaz et al. 2000; Mookherjee and Redfern 2002).

All far-infrared modes shift to higher frequency with increasing pressure, but distinct shifts in the pressure responses of different modes do occur. For example, the pressure shift of the band with an initial frequency of 112 cm^{-1} changes dramatically above 5–8 GPa, from $6.9 (\pm 0.39)\text{ cm}^{-1}/\text{GPa}$ below 5.1 GPa to $0.78 (\pm 0.12)\text{ cm}^{-1}/\text{GPa}$ at pressures above 7.8 GPa. As the 112 cm^{-1} band is generated by displacements of the interlayer K-ion, its shift in pressure is likely directly correlated with a reduction in the amount of compression taken up through interlayer compaction, which would be consistent with our observations of increased silicate stretching mode shifts at elevated pressures in the mid-infrared portion of the spectrum.

Also, the librational band near 408 cm^{-1} notably increases in its pressure shift near 5 GPa, from $0.75\text{ cm}^{-1}/\text{GPa}$ to $1.77 (\pm 0.08)$

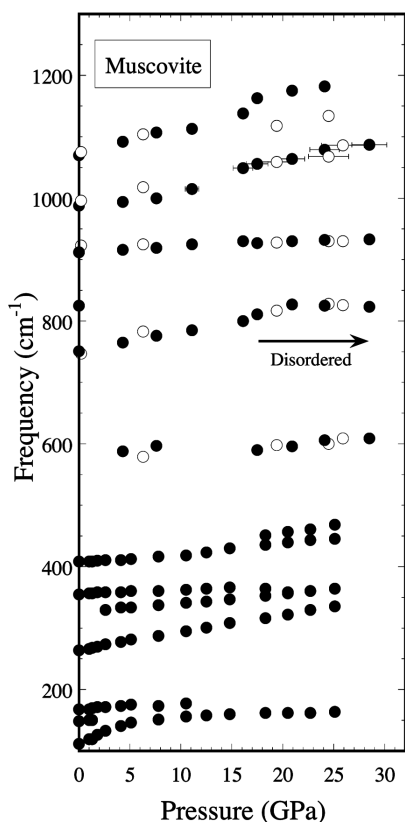


FIGURE 2. Mid- and far-infrared mode shifts of muscovite. The arrow denotes the range of pressures over which progressive disordering, culminating in X-ray amorphization, was observed by Faust and Knittle (1994). Solid symbols are on compression, open on decompression. Error bars in pressure for mid-infrared bands are shown for the band with initial frequency near 1000 cm^{-1} .

$\text{cm}^{-1}/\text{GPa}$; between 15 and 18 GPa, this peak also splits, with a clear high-frequency shoulder becoming present. Substantial intensity changes also take place between 4 and 20 GPa for bands between 250 and 355 cm^{-1} . The intensity of the band with an initial frequency near 325 cm^{-1} is notably enhanced at the expense of the band at 355 cm^{-1} , and a decrease in intensity of the 264 cm^{-1} band and corresponding increase in intensity of the $325/355\text{ cm}^{-1}$ band between 15 and 20 GPa occurs. It is possible that the intensity changes of these three bands may be associated with Fermi resonances, which can produce intensity changes in bands whose pressure shifts cause them to converge or cross at high pressures. Such Fermi resonances have been observed in other hydrous phases (e.g., Duffy et al. 1995; Knittle et al. 2001), and require that these bands be of the same symmetry; only two symmetry types of infrared-active vibrations exist in muscovite— A_u and B_u (e.g., McKeown et al. 1999a). However, while Fermi resonance might be invoked to explain the intensity changes occurring at high pressures in this portion of the far-infrared spectra (Fig. 1c), it clearly cannot explain the coalescence and broadening of the 325 and 355 cm^{-1} peaks between 15 and 18 GPa. Hence, the combination of this coalescence and the concomitant splitting of the 408 cm^{-1} band (each of which are consistent with a shift in symmetry and/or bonding environments) indicate that there is a structural change in muscovite near this pressure. The pressure range of 15–18 GPa for this structural change closely overlaps Faust and Knittle's (1994) observation of the onset of disordering within muscovite, and we hence associate these spectral changes (which also occur in tandem with band broadening: Fig. 1c) with disordering within the muscovite structure.

Figure 3 shows spectra of the hydroxyl-stretching vibration of muscovite under compression and decompression, and Figure 4a shows the corresponding shift with pressure. The vibration has a highly non-linear shift to 20 GPa. A quadratic fit to the frequency of this vibration (Table 1) to 16.1 GPa yields a small pressure shift at zero pressure: $-0.06\text{ cm}^{-1}/\text{GPa}$. The shift to lower frequency rapidly increases with pressure to values of $\sim -20\text{ cm}^{-1}/\text{GPa}$ between 16.1 and 17.5 GPa. While shifts to lower frequency with pressure are common among hydrogen-bonded O-H stretching vibrations, and simply reflect an increase in hydrogen bonding under pressure as expected for compression of O-H...O distances, highly non-linear shifts are unusual. At pressures above 17 GPa, the character of the hydroxyl bond changes dramatically. The band broadens by a factor of 3 (Fig. 4b) and its shift becomes dramatically smaller. Clearly, the nature of the hydroxyl band and its pressure response undergo discontinuous changes near this pressure. The process is reversible on decompression, albeit with hysteresis (Fig. 3b).

For reference, the zero-pressure hydroxyl bond location in the muscovite crystal structure lies close to within the *a-b* plane, with neutron diffraction yielding an angle of 12° (Rothbauer 1971) or 6° (Catti et al. 1994) for this bond relative to the *a-b* plane. These neutron characterizations are in excellent agreement with measurements of the pleochroic hydroxyl-stretching vibration, which yield constraints on the average orientation of the hydroxyl dipole moment (e.g., Vedder and McDonald 1963). There are also indications from neutron spectroscopy at 12 K that two independent, but closely separated, hydroxyl sites are present within muscovite, lowering the symmetry of muscovite

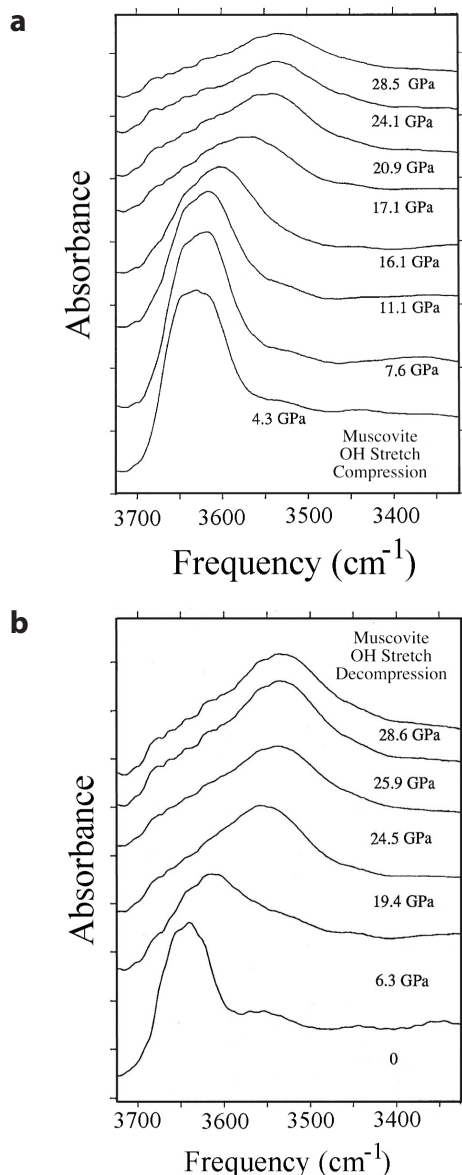


FIGURE 3. (a) Spectra of the hydroxyl-stretching vibration of muscovite on compression; (b) spectra of the hydroxyl-stretching vibration of muscovite on decompression.

and with the occupancy of the H atoms over the two sites involving long-range ordering (Liang et al. 1998). This two-site model is consistent with interpretations of the infrared spectrum of muscovite (Serratos and Bradley 1958; Rouxhet 1970) and with electrostatic calculations (Abbott et al. 1989; Liang and Hawthorne 1998). Recently, Gatta et al. (2011) have presented neutron diffraction of muscovite at 20 K that is consistent with a single hydroxyl site; yet, Abbott et al. (1989) have noted that the occupancy of the two sites may be heavily affected by the local distribution of aluminum and silicon cations. The possible two-site configuration is shown in Figure 5: the position of the H1 atom in the structure is very close to neutron refinements of the muscovite structure that incorporate only a single hydrogen site (Rothbauer 1971; Catti et al. 1994). The key point here is

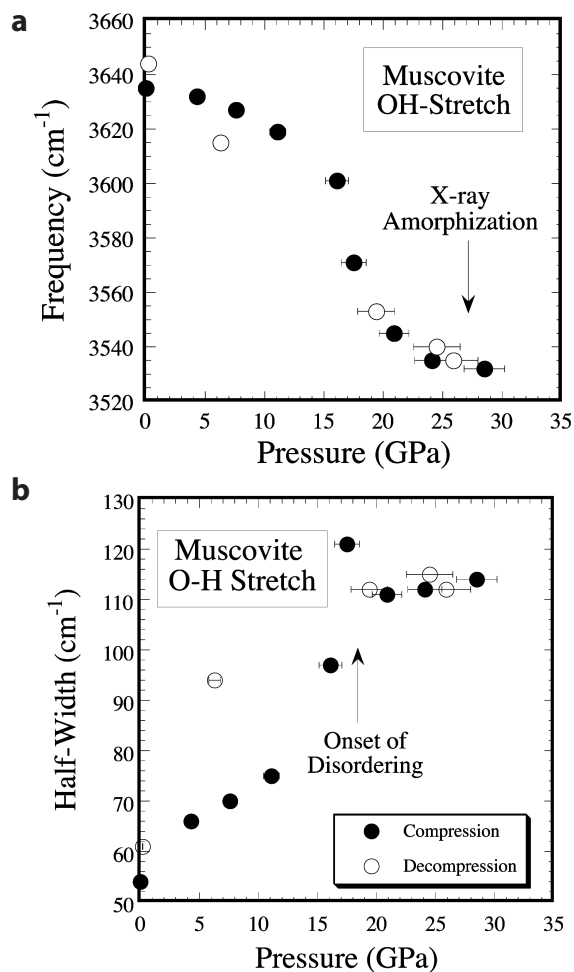


FIGURE 4. (a) Mode shift of the hydroxyl-stretching vibration of muscovite; (b) peak-width of the hydroxyl-stretching vibration of muscovite. Pressures of the onset of disordering and of X-ray amorphization (vertical arrows) are from Faust and Knittle (1994).

that, in muscovite at ambient pressures, there may be multiple occupied hydrogen sites: that there could be additional hydrogen sites that become occupied at high pressures (with accompanying disorder across the sites) would be consistent with our infrared data, and the observations of high-pressure disordering of this structure prior to X-ray amorphization (e.g., Faust and Knittle 1994; Gatta et al. 2010).

The H1-associated hydroxyl can be viewed as having a weak trifurcated hydrogen bond with the O5, O4, and O2 anions within the structure (the O2 is a basal oxygen, while the O4 and O5 are apical). At zero pressure, each of these anions lies between 2.62 and 2.67 Å from the H1-hydrogen, with O-H...O angles between 135° and 139.7° (Catti et al. 1994). At ambient pressure, the frequency of the hydroxyl-stretching vibration is chemically modulated primarily by the identity of the octahedral cation and the degree of underbonding in the apical O atoms (Besson and Drits 1997; Martinez-Alonso et al. 2002). That the Si1 site lies 2.985 Å from the hydrogen, with an O-H...Si angle of 134.8°, is also important from an electrostatic viewpoint (Geise 1979; Brigatti et al. 1998). The hydroxyl orientation is initially con-

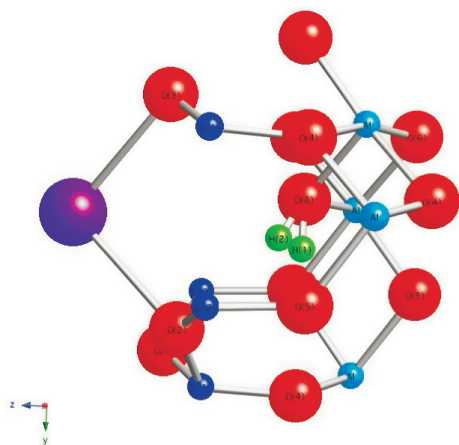


FIGURE 5. Local environment of the two possible hydroxyl sites in muscovite at ambient pressure. Atomic locations are from Liang et al. (1998). This image is down the *a-b* plane of the structure; the *c*-axis is horizontal in this figure. (Color online.)

trolled by its pointing toward the vacant octahedral site, which minimizes cation-hydrogen repulsion (e.g., Geise 1979). There are additional hints that notable changes in hydroxyl orientation may accompany compression. Neutron results at 2 GPa (Catti et al. 1994) suggest that the hydrogen location moves further out of the *a-b* plane and toward the interlayer cation (from 6 to 12° from 0 to 2 GPa, or 84 to 78° relative to the *c*-axis). Yet, the decreases in hydrogen bond distances that produce the shift to lower frequency of the hydroxyl vibration may be directly correlated with increases in the ditrigonal rotation angle (α) of the tetrahedra, which has been shown to increase under pressure (Comodi and Zanazzi 1995).

The most parsimonious interpretation of our data on the infrared spectra of muscovite suggests three compressional regimes. First, up to ~8 GPa, compression is dominated by shifts in interlayer spacing. This is in accord with single-crystal X-ray diffraction data on muscovite that extend to 3.8 GPa (Comodi and Zanazzi 1995) and density functional calculations to 6 GPa (Ortega-Castro et al. 2010), which show that the compressibility in the *c*-direction is about a factor of 5 greater than that in the *a-b* plane. At pressures above ~8 GPa, the dramatic change in pressure dependence of the K-O stretching vibration implies that the compressibility of the interlayer spacing may be notably reduced: hints of such a change in the compressibility of the *c*-axis are present in the polycrystalline diffraction data of Curetti et al. (2006).

At pressures from 8 to ~17 GPa, we propose that the rapid increase in hydrogen bonding in this pressure interval relative to lower pressures (e.g., Fig. 4a) is associated with increased compaction of the O-H...O distances within the vacant octahedral sites. This compaction associated with the vacant octahedral site (manifested by the increased H-bonding), and likely of other structural units within the layers, becomes progressively more important in the bulk compression of the crystal within this pressure range—particularly as the interlayer compressibility is notably reduced. That enhanced intralayer compaction occurs is

consistent with the non-linear shift of the Si-O (basal) stretching vibration at ~1000 cm^{-1} , for which the mode shift abruptly increases above 8 GPa (Fig. 2). This steeper pressure shift of the basal Si-O stretching band implies that continued compaction along the *c*-axis produces an increased effect on the Si-O bonds that are juxtaposed with the K-cations in this pressure range. It is possible that this may be associated with pressure-induced shifts in the O(basal)-T-O(basal) angle, which is in turn correlated with the degree of corrugation of the tetrahedral sheet (Ortega-Castro et al. 2010).

Above 17 GPa, the aberrant broadening and change in pressure-shift of the hydroxyl-stretching vibration occurs, and a new mode that lies close to an O-H libration also appears. Notably, throughout the pressure range to 30 GPa, the coordination number of the tetrahedral cations appears to remain at 4: the tetrahedral peaks remain strong within muscovite, and no new infrared peaks in the 600–900 cm^{-1} range that might be associated with higher coordination of initially tetrahedral cations appear. Thus, no distortions that produce higher coordination defects appear to occur in this pressure range, as occurs near the amorphization pressure in both framework silicates and germanates (quartz, coesite, feldspars) and orthosilicates (e.g., fayalite) (Itie et al. 1989; Williams and Jeanloz 1989; Williams et al. 1990, 1993; Williams 1998). Nevertheless, the increase in peak width of both the tetrahedral-stretching and hydroxyl-stretching peaks at the higher pressures of this study implies that both of these environments undergo disordering under compression. We speculate that the disordering of the hydroxyl environment involves the development of stronger, and probably more directional, hydrogen bonds with one of the three almost-equidistant tetrahedrally cation-bound O atoms available for hydrogen-bonding by each hydrogen. This prospective threefold positional option for each hydrogen could produce long-range hydrogen disorder, and associated distortions of the tetrahedra produced by the onset of stronger hydrogen bonding. In this sense, the disordering and ultimate X-ray amorphization of muscovite may have considerable commonality with that of $\text{Ca}(\text{OH})_2$ and $\text{Co}(\text{OH})_2$ (Raugei et al. 1999; Parise et al. 1999). At a minimum, additional hydrogen sites likely become energetically preferable above 17 GPa, and occupancy of these different sites produces long-range disordering of the crystal: a result akin to the possible bifurcation of the H-sites at zero-pressure (Liang et al. 1998).

Mode Grüneisen parameters of muscovite

The bulk thermodynamic Grüneisen parameter of muscovite can be calculated from $\alpha K_s / \rho C_p$, where α is the thermal expansion, K_s the adiabatic bulk modulus, ρ the density, and C_p the heat capacity. Utilizing a value of $3.57 \times 10^{-5}/\text{K}$ for the ambient pressure and temperature thermal expansion (e.g., Comodi et al. 2002), an adiabatic bulk modulus of 58.2 GPa (Vaughan and Guggenheim 1986), a density of 2830 kg/m^3 , and a 300 K heat capacity of 330 $\text{J}/(\text{mol}\cdot\text{K})$ (Krupka et al. 1979) yield a Grüneisen parameter of 0.89. To provide a more complete data set for comparison with the thermodynamic Grüneisen parameter, a reconnaissance study of the Raman spectrum of muscovite under pressure was conducted; previously, two Raman modes of muscovite had been observed to pressures of 2 GPa (Holtz et al. 1993). The mode shifts for four Raman modes and representative

Raman spectra are shown in Figure 6, and our aggregate mode shift data from the combination of mid-infrared, far-infrared, and Raman data are shown in Table 1. Mode Grüneisen parameters are calculated from $K_T(d\omega/dP)/\omega_0$, where K_T is the isothermal bulk modulus (taken as 60 GPa from the static compression studies of Faust and Knittle 1994 and Comodi and Zanazzi 1995). The average of the 18 vibrational modes characterized (17 from this study, 1 from Holtz et al. 1993) produces an average Grüneisen parameter of the observed vibrational modes of 0.54; this value is substantially less than the thermochemical value.

The individual mode values are, for the most part, generally close to the Grüneisen parameters determined from thermal mode shifts from high-temperature spectra of muscovite at ambient pressure (Zhang et al. 2010), with the important exceptions of the K-translation mode at 112 cm^{-1} and the O-H stretching vibration. The K-translation has a thermal mode Grüneisen parameter of 0.97, in contrast to the pressure-determined value of 3.70, and the hydroxyl stretch thermal mode Grüneisen parameter is +0.07, which differs in sign from our value of -0.001 (Table 1; Zhang et al. 2010). Thus, it appears that the structural changes in muscovite associated with the K-site and the hydroxyl unit produced by thermally induced volume changes differ substantially from those produced through pressure-induced volume changes. Indeed, the hydrogen bonds and the K-O bonds are the weakest nearest-neighbor bonding interactions within the muscovite structure, and the differences between thermal expansion and compaction appear to be most acute for these weakly bonded interactions.

Perhaps the most notable aspect of the average of the pressure-determined mode Grüneisen parameters is that despite the number of vibrations characterized, the single far-infrared vibration associated with K-translations contributes 35% of the vibrational value, or 0.19 out of 0.54 of the average vibra-

tional Grüneisen parameter. Hence, the thermodynamic value is likely modulated by a small number of highly pressure-sensitive modes, of which we have sampled only a single one. Indeed, of the 111 optic vibrations predicted by factor group analysis (e.g., McKeown et al. 1999a), our measurements sample only 17 (although a portion of these likely incorporate overlapping, and similarly shifting, bands). Yet, a single one of the six vibrations likely associated with K-translations is sampled, and our results may disproportionately under-sample vibrations primarily associated with octahedral translations (Table 1). Thus, the important observation here is that much of the thermodynamic Grüneisen parameter, and hence the vibrational anharmonicity of muscovite, may be primarily generated from a few strongly pressure-dependent optic vibrations.

Biotite

To assess the relative effect of pressure on hydroxyl units in dioctahedral and trioctahedral environments, we characterized the mid-infrared spectrum of biotite from Bancroft, Ontario. Our rationale for selecting this composition is that the hydroxyl-stretching region of this biotite is comparatively simple relative to that of most biotites, with two well-defined bands associated with O-H units: one attributable to the trioctahedral site, and the other a "V" site associated with a dioctahedral-type environment with a vacancy in the octahedral layer (Fripiat et al. 1965; Rouxhet 1970; Chaussidon 1972).

The mid-infrared spectral region on both compression and decompression is shown in Figures 7a and 7b, the hydroxyl mode spectra in Figure 7b, with mode shifts shown in Figure 8 and tabulated with assignments in Table 2 (Vedder 1964; Boukili et al. 2003). The lower pressure mid-infrared spectra have some degree of fringing, but the major spectral features are clearly identifiable: our ambient-pressure peak locations agree well with prior measurements on biotite (Liese 1963; Vedder 1964). As with muscovite, most of the bands shift to higher frequency with pressure: the O-H libration has, however, a shift that is indistinguishable from zero. The shifts of the mid-infrared bands in biotite closely mirror those of the corresponding bands in muscovite (Tables 1 and 2). However, the bands in biotite both broaden more at high pressures and lower amplitude features become unresolvable. Indeed, above ~20 GPa only three spectral bands are resolvable, and at the highest pressures of these measurements there is both an apparent weakening of the tetrahedral stretching bands and an increased spectral amplitude between 650 and 900 cm^{-1} (Fig. 7a). Hence, it is possible that within this biotite composition, a portion of the tetrahedral cations begin to be destabilized above ~20 GPa. This general shift in infrared amplitude is similar to that observed in the infrared spectra of polymerized silicates upon pressure-induced amorphization (Williams et al. 1993; Williams 1998), and this spectral shift has been associated with a shift in tetrahedral cation coordination (e.g., Meade et al. 1993). Regardless of the origin of this shift in amplitude, the overall infrared spectrum of this material becomes notably simpler between ~16 and 20 GPa, with only three peaks being readily tracked, and it is possible that this is induced by a structural change within this pressure range. By analogy with the spectral broadening observed to occur in muscovite at high pressures within the mid-infrared region, the broadening and

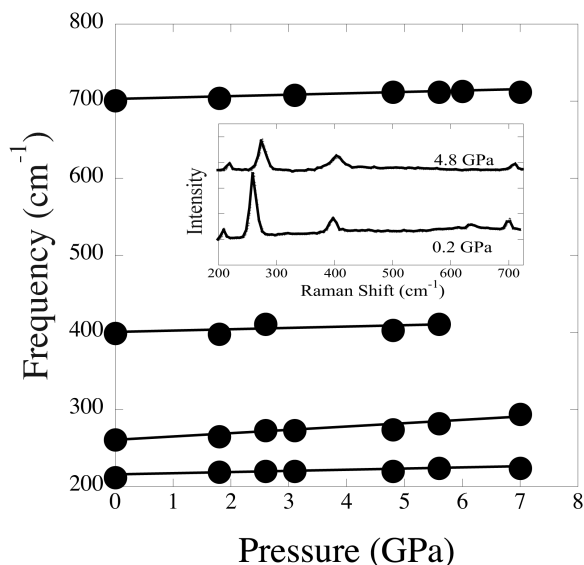


FIGURE 6. Mode shifts of the most intense Raman bands of muscovite. Inset shows representative Raman spectra of muscovite under pressure: methanol:ethanol peaks have been subtracted from the spectra.

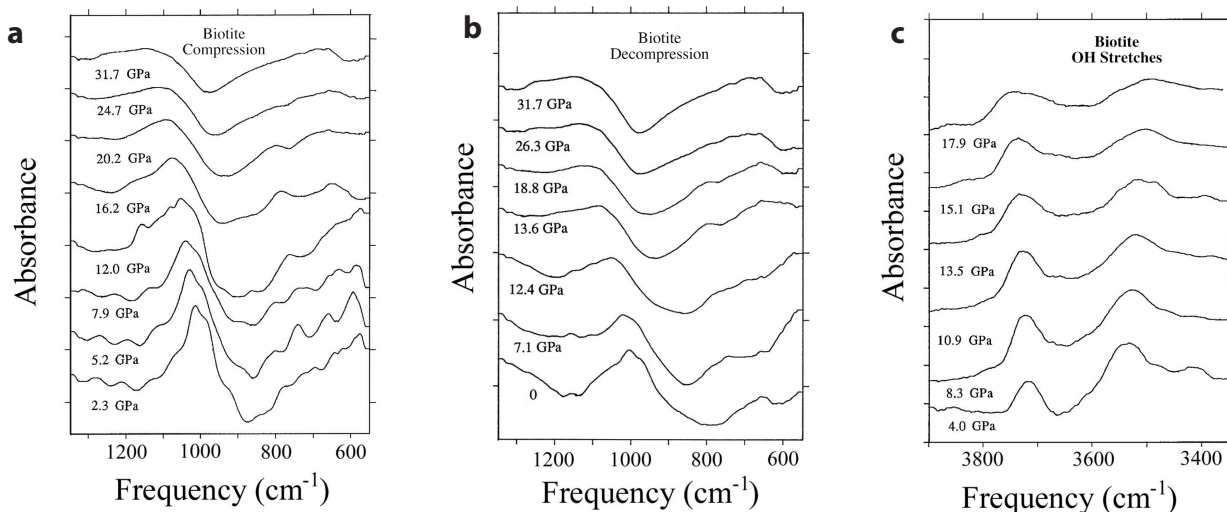


FIGURE 7. (a) Mid-infrared spectra of biotite on compression; (b) spectra of biotite on decompression; (c) spectra of the hydroxyl-stretching vibrations of biotite at high pressures. The lower frequency peak is associated with a hydroxyl unit that is juxtaposed with an octahedral vacancy.

TABLE 2. Mode shifts and assignments of the infrared spectrum of biotite

ν_0 (cm^{-1})	Pressure shift ($\text{cm}^{-1}/\text{GPa}$)	σ	Assignment
3703	2.05	0.23	O-H Stretch
3555	-2.82	0.35	O-H Stretch (Oct. Vacancy)
1008	4.10	0.08	T-O Stretch
975	3.29	0.05	T-O(basal) Stretch
721	3.54	0.34	T(Si,Al)-O-T(Si) Bend
619	1.94	0.14	T(Al)-O-T(Si) Bend
582	0.07	0.48	O-H Libration

Note: Hydroxyl vibration shifts are fits to results below 13.5 GPa.

disappearance of low-amplitude features in biotite in this pressure range may be associated with the onset of lattice disordering in this material. Destabilization of tetrahedral cations may commence above ~ 20 GPa, where a general increase in spectral amplitude between 650 and 900 cm^{-1} begins to occur.

Our spectra in the hydroxyl region (Figs. 7c and 8b) agree well with previous measurements of the infrared spectra of the hydroxyl vibrations in biotite from the Bancroft locale (Fripiat et al. 1965; Rouxhet 1970). The hydroxyl vibrations of this biotite are generated from a hydroxyl in a trioctahedral environment (the band with a zero-pressure frequency near 3703 cm^{-1}) and a band associated with hydroxyls juxtaposed with a vacancy in the octahedral sites (the 3555 cm^{-1} band: a dioctahedral-like environment) (e.g., Vedder 1964; Rouxhet 1970; Robert and Kodama 1988; Redhammer et al. 2000). Clearly, the higher-lying trioctahedrally associated band shifts to higher frequency on compression. Such pressure-induced shifts to higher frequency are not unusual for hydroxyl-stretching vibrations located above ~ 3600 cm^{-1} in silicates, having previously been observed in minerals as structurally diverse as topaz, talc, and other layer silicates (e.g., Holtz et al. 1993; Johnston et al. 2002; Bradbury and Williams 2003; Scott et al. 2007; Parry et al. 2007). In the case of the trioctahedral environment in micas, the shift of the hydroxyl vibration to higher frequency (which has also been observed in Raman experiments to 2 GPa on phlogopite: Holtz et al. 1993) is almost certainly associated with repulsion be-

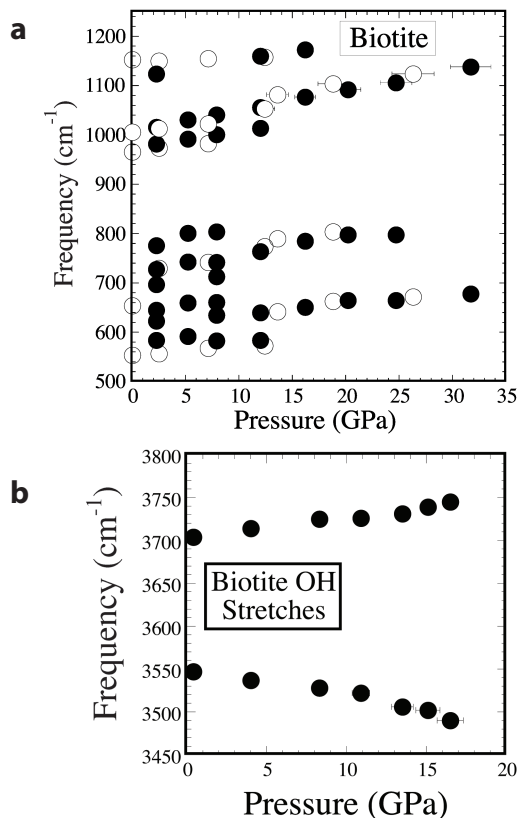


FIGURE 8. (a) Mid-infrared mode shifts of biotite at high pressures. Error bars in pressure are shown on the peak occurring at ~ 1000 cm^{-1} . (b) Mode shifts of the hydroxyl bands of biotite under pressure.

tween the interlayer alkali cation and the hydroxyl unit. Within trioctahedral micas, the hydroxyl unit lies almost normal to the a - b plane, and points nearly directly toward the alkali cation (e.g., Bailey 1984). Indeed, for the 3703 cm^{-1} band, the effect of hydrogen-alkali repulsion entirely counterbalances any enhancement in hydrogen bonding with pressure that is produced by

closer approaches of O-H...O distances under compression. At the highest pressures of these measurements, this trioctahedral band broadens significantly to its low-frequency side, implying that there may be increased positional disorder of the H-location in the trioctahedral environment at high pressure, with some environments having somewhat stronger H-bonding (Fig. 7c).

The behavior of the "V," or vacancy, band (using the nomenclature of Vedder 1964) with an initial frequency of 3555 cm^{-1} shows an increasingly large shift to lower frequency with pressure (Fig. 8b), in a manner generally similar to that of the hydroxyl-stretching vibration in muscovite (Fig. 4a). The location of the O-H bond axes relative to the *a-b* plane in biotite has been examined using infrared pleochroic experiments that provide a constraint on the orientation of the O-H dipole moment (Vedder 1964). For the V band, the O-H group appears (as in muscovite) to lie close to within the *a-b* plane and is probably pointed toward the vacant octahedral site generated by the incomplete occupancy of the octahedral sites in this biotite (Vedder 1964). Under pressure, the shift to lower frequency is certainly produced by an enhancement of hydrogen bonding under pressure; such an increase in hydrogen bonding is likely associated with a compaction of the distance between the O atoms associated with the vacant site and the hydrogen atom. At the highest pressures of the measurements, the V band also broadens considerably, but it does not (over the pressure range to 17 GPa) undergo the nearly discontinuous shift undergone by the comparable band in muscovite.

Under metastable compression, biotite thus appears to undergo some level of disordering in the 16–20 GPa range, as manifested both by the behavior of the silicate bending and stretching bands, as well as the broadening of the hydroxyl bands. At pressures above ~20 GPa, some tetrahedral units may begin to distort to more highly coordinated environments. Therefore,

although there is no X-ray data on compression for this compound, we speculate that it may become amorphous to X-rays in the 25–30 GPa pressure range.

Phlogopite

To provide a comparison with a purely trioctahedral mica, a reconnaissance study was conducted of the infrared spectrum of phlogopite under pressure. Representative mid-infrared spectra and spectra of the hydroxyl region of phlogopite are shown in Figure 9, with pressure shifts shown in Figure 10 and tabulated in Table 3. Our zero-pressure phlogopite results agree well with prior determinations of the infrared spectrum of this material, and we utilize assignments in Table 3 from these prior studies of the ambient pressure spectrum of phlogopite (e.g., McKeown et al. 1999b; Jenkins 1989; Vedder 1964). The infrared peaks associated with tetrahedral stretching and T-O-T bending vibrations in phlogopite shift similarly to those of biotite and muscovite, with the sole exception of the peak with a zero-pressure frequency of 602 cm^{-1} , which has a small shift to lower frequency with compression. This band is probably associated with a libration of the hydroxyl group, as such vibrations typically have small or negative pressure shifts (e.g., Williams and Guenther 1996; Bradbury and Williams 2003; Scott et al. 2007). Although some broadening of the phlogopite bands occurs under compression, this broadening is reversible on decompression (Fig. 9b) and, unlike biotite, the region between 650 and 900 cm^{-1} does not increase in amplitude over this pressure range.

The single hydroxyl-stretching band shifts to higher wavenumber at a somewhat more rapid rate than the corresponding

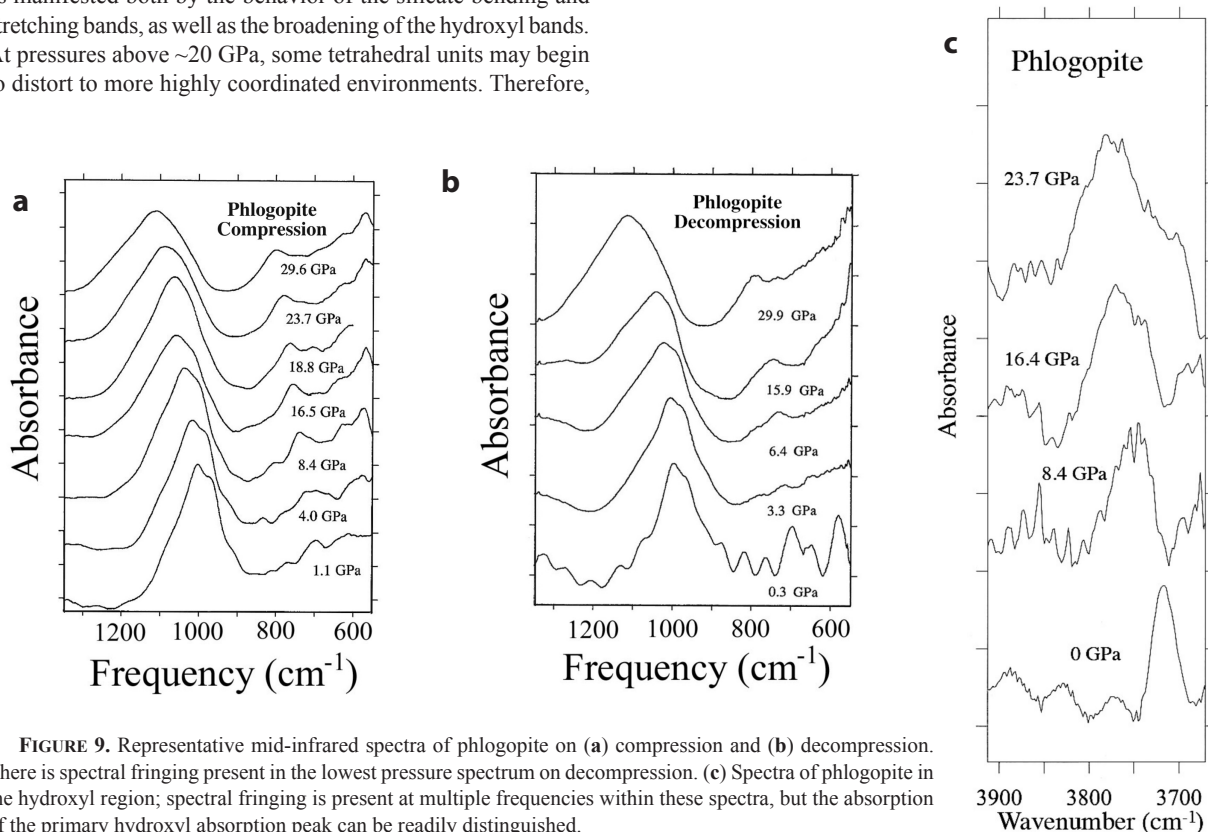


FIGURE 9. Representative mid-infrared spectra of phlogopite on (a) compression and (b) decompression. There is spectral fringing present in the lowest pressure spectrum on decompression. (c) Spectra of phlogopite in the hydroxyl region; spectral fringing is present at multiple frequencies within these spectra, but the absorption of the primary hydroxyl absorption peak can be readily distinguished.

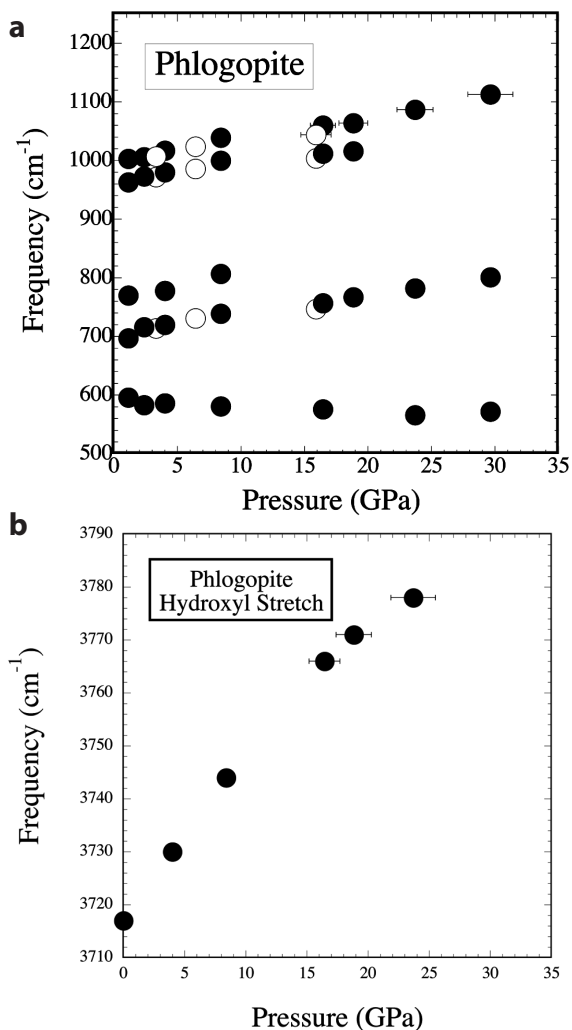


FIGURE 10. (a) Mode shifts of the mid-infrared bands of phlogopite; error bars are shown on the ~ 1000 cm^{-1} band. Solid symbols are on compression and open symbols on decompression. (b) Shift of the hydroxyl band of phlogopite.

TABLE 3. Mode shifts and assignments of the infrared spectrum of phlogopite

ν_0 (cm^{-1})	Pressure shift ($\text{cm}^{-1}/\text{GPa}$)	σ	Assignment
3717	3.78	0.18	O-H Stretch
1000	3.71	0.20	T-O Stretch
966	2.94	0.43	T-O(basal) Stretch
703	3.41	0.30	O-H Libration
619	1.94	0.14	T(Si,Al)-O-T(Si) Bend
594	-0.59	0.19	T(Al)-O-T(Si) Bend

trioctahedral hydroxyl stretch of biotite (Figs. 9c and 10b). A definitive origin of this difference in pressure shift between biotite and phlogopite is difficult to determine, but the precise identity of the octahedral cations plays a major role in determining the zero-pressure hydroxyl peak location in micas (e.g., Velde 1983; Robert and Kodama 1988; Besson and Drits 1997; Martinez-Alonso et al. 2002). Hence, it is possible that the enhanced compressibility of the Mg-bearing octahedra (relative to micas containing Al-bearing octahedra, such as biotite) may

produce the higher pressure shift: this may be a consequence of an increased mismatch at pressure between the octahedral and tetrahedral layers, which is known to produce tetrahedral rotation and corresponding shifting of oxygen anions (Bailey 1984; Ferraris and Ivaldi 2002).

Spectroscopic constraints on the relative response to compression of dioctahedral and trioctahedral micas

Hydroxyl units within dioctahedral micas, and those with dioctahedral sites, undergo increases in hydrogen bonding with pressure. In the case of muscovite, an abrupt pressure-induced shift in hydrogen bonding is intimately tied to the pressure at which crystalline X-ray diffraction from this material is lost. While the manifestations of this transition are most clearly apparent in the hydroxyl portion of the spectrum (both librational and stretching vibrations), it may also have a net effect on the pressure shift of the Al-O-Si bending modes as well. Far-infrared spectra indicate that the compressibility of the interlayer region notably decreases in muscovite above ~ 5 – 8 GPa, and above this pressure, intra-layer deformation may begin to play a progressively larger role in the compression of this material. Biotite, with a combination of dioctahedral and trioctahedral sites, appears to be becoming disordered at the highest pressures of our measurements (30 GPa), while phlogopite appears to be the least altered of these three micas by extreme metastable compression.

Hence, the differing responses to pressure of the dioctahedral and trioctahedral environments appear to be modulated by the interplay between the orientation of the hydrogen ion and the presence of the vacant octahedral site. The dioctahedral hydroxyl is oriented almost in the a - b plane toward the vacant octahedral site, and its disordering within muscovite is likely associated with it ultimately forming multiple hydrogen bonds within the vacant octahedron (at ambient pressure in muscovite, the hydrogen is at modestly different distances from three different hydrogen atoms within the structure (Rothbauer 1971; Catti et al. 1994), and there may be two sites that lie close to one another in which a given hydrogen might reside (Liang et al. 1998). We speculate that directional, but aperiodic, hydrogen bonds are formed with different oxygen ions within muscovite near its pressure of X-ray amorphization, and that this onset of weakly hydrogen-bound environments may induce local and aperiodic distortions of the vacant octahedral site within the structure.

In contrast to the hydrogen-bond strengthening undergone by the dioctahedral environments in micas, the response of hydroxyl-stretching vibrations associated with trioctahedral configurations is to move to higher frequencies, likely in response to the electrostatic repulsion between the alkali interlayer cation and the hydrogen atom. Indeed, this orientation of the hydroxyl unit (in which the hydrogen lies close to along the [001] direction, and roughly equidistant from basal O atoms of the tetrahedral layer) may serve to stabilize the trioctahedral structure relative to the loss of crystallinity observed in muscovite. Considerable discussion has been devoted to the possibility that increases in the tetrahedral rotation angle, α , which is known to increase with pressure as a consequence of differential compressibility of the tetrahedral and octahedral layers, may affect the stability of the mica structure (Ferraris and Ivaldi 2002; Ortega-Castro et al. 2010). It is possible that this might be an important effect

over the pressure range of our experiments but, unlike the clear role of the hydroxyl unit in disordering of these materials, our data do not directly constrain whether this is the case. Thus, a coordination instability of the tetrahedra at the highest pressure in biotite may be driven by large values of α being reached, with layer mismatches and associated polyhedral distortions being associated with an incipient coordination change in the tetrahedral layer.

ACKNOWLEDGMENTS

Work supported by the U.S. NSF, including partial support by COMPRES through NSF cooperative agreement 06-49658. We are grateful to two anonymous reviewers for helpful and constructive comments.

REFERENCES CITED

- Abbott, R.N. Jr., Post, J.E., and Burnham, C.W. (1989) Treatment of hydroxyl in structure-energy calculations. *American Mineralogist*, 74, 141–150.
- Bailey, S.W. (1984) Crystal chemistry of the true micas. In S.W. Bailey, Ed., *Micas*, 13, p. 13–60. Reviews of Mineralogy, Mineralogical Society of America, Chantilly, Virginia.
- Besson, G. and Drits, V.A. (1997) Refined relationships between chemical composition of dioctahedral fine-grained micaceous minerals and their infrared spectra within the OH stretching region. Part II: the main factors affecting OH vibrations and quantitative analysis. *Clays and Clay Minerals*, 45, 170–183.
- Boukili, B., Holtz, F., Beny, J.-M., Abdelouafi, A., and Niazi, S. (2003) Infrared spectra of annite in the interlayer and lattice vibrational range. *Schweizerische Mineralogische und Petrographische Mitteilungen*, 83, 33–46.
- Bradbury, S. and Williams, Q. (2003) Contrasting bonding behavior of two hydroxyl-bearing metamorphic minerals under pressure: Clinozoisite and topaz. *American Mineralogist*, 88, 1460–1470.
- Brigatti, M.F., Frigieri, P., and Poppi, L. (1998) Crystal chemistry of Mg-, Fe-bearing muscovites- $2M_1$. *American Mineralogist*, 83, 775–783.
- Butler, I.S. and Frost, R.L. (2006) An overview of the high-pressure vibrational spectra of clays and related minerals. *Applied Spectroscopy Reviews*, 41, 449–471.
- Catti, M., Ferraris, G., Hull, S., and Pavese, A. (1994) Powder neutron diffraction study of $2M_1$ muscovite at room pressure and at 2 GPa. *European Journal of Mineralogy*, 6, 171–178.
- Chaussidon, J. (1972) The IR spectrum of structural hydroxyls of K-depleted biotites. *Clays and Clay Minerals*, 20, 59–67.
- Chon, C.M., Kim, S.A., and Moon, H.S. (2003) Crystal structures of biotite at high temperatures and of heat-treated biotite using neutron powder diffraction. *Clays and Clay Minerals*, 51, 519–528.
- Comodi, P., Fumagalli, P., Montagnoli, M., and Zanazzi, P.F. (2004) A single-crystal study on the pressure behavior of phlogopite and petrological implications. *American Mineralogist*, 89, 647–653.
- Comodi, P., Gatta, G.D., Zanazzi, P.F., Levy, D., and Crichton, W. (2002) Thermal equations of state of dioctahedral micas on the join muscovite-paragonite. *Physics and Chemistry of Minerals*, 29, 538–544.
- Comodi, P. and Zanazzi, P.F. (1995) High-pressure structural study of muscovite. *Physics and Chemistry of Minerals*, 22, 170–177.
- Curetti, N., Levy, D., Pavese, A., and Ivaldi, G. (2006) Elastic properties and stability of coexisting 3T and $2M_1$ phengite polytypes. *Physics and Chemistry of Minerals*, 32, 670–678.
- Dera, P., Prewitt, C.T., Japel, S., Bish, D.L., and Johnston, C.T. (2003) Pressure-controlled polytypism in hydrous layered materials. *American Mineralogist*, 88, 1428–1435.
- Diaz, M., Farmer, V.C., and Prost, R. (2000) Characterization and assignment of far infrared absorption bands of K^+ in muscovite. *Clays and Clay Minerals*, 48, 433–438.
- Domanik, K.J. and Holloway, J.R. (1996) The stability and composition of phengitic muscovite and associated phases from 5.5 to 11 GPa: Implications for deeply subducted sediments. *Geochimica et Cosmochimica Acta*, 60, 4133–4150.
- Downes, H., MacDonald, R., Upton, B.G.J., Cox, K.G., Bodinier, J.-L., Mason, P.R.D., James, D., Hill, P.G., and Hearn, B.C. Jr. (2004) Ultramafic xenoliths from the Bearpaw Mountains, Montana, USA: Evidence for multiple metasomatic events in the lithospheric mantle beneath the Wyoming craton. *Journal of Petrology*, 45, 1631–1662.
- Duffy, T.S., Meade, C., Fei, Y.W., Mao, H.K., and Hemley, R.J. (1995) High-pressure phase transition in brucite, $Mg(OH)_2$. *American Mineralogist*, 80, 222–230.
- Farmer, V.C. (1974) The layer silicates. In V.C. Farmer, Ed., *The Infrared Spectra of Minerals*, p. 331–363. Mineralogical Society, London.
- Faust, J. and Knittle, E. (1994) The equation of state, amorphization, and high-pressure phase diagram of muscovite. *Journal of Geophysical Research*, 99, 19785–19792.
- Ferraris, G. and Ivaldi, G. (2002) Structural features of micas. In A. Mottana, F.P. Sassi, J.B. Thompson Jr., and S. Guggenheim, Eds., *Micas: Crystal Chemistry and Metamorphic Petrology*, 46, p. 117–153. Reviews in Mineralogy and Geochemistry, Mineralogical Society of America, Chantilly, Virginia.
- Fripiat, J.J., Rouxhet, P., and Jacobs, H. (1965) Proton delocalization in micas. *American Mineralogist*, 50, 1937–1958.
- Gatta, G.D., Rotiroli, N., Lotti, P., Pavese, A., and Curetti, N. (2010) Structural evolution of a $2M_1$ phengite mica up to 11 GPa: An in situ single-crystal X-ray diffraction study. *Physics and Chemistry of Minerals*, 37, 581–591.
- Gatta, G.D., McIntyre, G.J., Sassi, R., Rotiroli, N., and Pavese, N. (2011) Hydrogen-bond and cation partitioning in muscovite: A single-crystal neutron-diffraction study at 295 and 20 K. *American Mineralogist*, 96, 34–41.
- Geise, R.F. Jr. (1979) Hydroxyl orientations in 2:1 phyllosilicates. *Clays and Clay Minerals*, 27, 213–223.
- Hirschmann, M.M. (2006) Water, melting and the deep Earth H_2O cycle, *Annual Review of Earth and Planetary Science*, 34, 629–653.
- Holtz, M., Solin, S.A., and Pinnavaia, T.J. (1993) Effect of pressure on the Raman vibrational modes of layered aluminosilicate compounds. *Physical Review B*, 48, 13312–13317.
- Itie, J.P., Polian, A., Calas, G., Petiau, J., Fontaine, A., and Tolentino, H. (1989) Pressure-induced coordination changes in crystalline and vitreous GeO_2 . *Physical Review Letters*, 63, 398–401.
- Jenkins, D.M. (1989) Empirical study of the infrared lattice vibrations (1100–350 cm^{-1}) of phlogopite. *Physics and Chemistry of Minerals*, 16, 408–414.
- Johnston, C.T., Wang, S.-L., Bish, D.L., Dera, P., Agnew, S.F., and Kenney, J.W. (2002) Novel pressure-induced phase transformations in hydrous layered material. *Geophysical Research Letters*, 29, 171–174.
- Klotz, S., Chervin, J.-C., Munsch, P., and LeMarchand, G. (2009) Hydrostatic limits of 11 pressure transmitting media. *Journal of Physics D Applied Physics*, 42, 075413.
- Knittle, E., Phillips, W., and Williams, Q. (2001) An infrared and Raman spectroscopic study of gypsum at high pressures. *Physics and Chemistry of Minerals*, 28, 630–640.
- Krupka, K.M., Robie, R.A., and Hemingway, B.S. (1979) High-temperature heat capacities of corundum, periclase, anorthite, $CaAl_2Si_2O_8$ glass, muscovite, pyrophyllite, $KAlSi_3O_8$ glass, grossular, and $NaAlSi_3O_8$ glass. *American Mineralogist*, 64, 86–101.
- Langer, K., Chatterjee, N.D., and Abraham, K. (1981) Infrared studies of some synthetic and natural $2M_1$ dioctahedral micas. *Neues Jahrbuch für Mineralogische Abhandlungen*, 142, 91–110.
- Liang, J.J. and Hawthorne, F.C. (1998) Calculated H-atom positions in micas and clay minerals. *Canadian Mineralogist*, 36, 1577–1585.
- Liang, J.J., Hawthorne, F.C., and Swainson, I.P. (1998) Triclinic muscovite: X-ray diffraction, neutron diffraction and photo-acoustic FTIR spectroscopy. *Canadian Mineralogist*, 36, 1017–1027.
- Liese, H.C. (1963) Tetrahedrally coordinated aluminum in some natural biotites: An infrared absorption analysis. *American Mineralogist*, 48, 980–990.
- Loh, E. (1973) Optical vibrations of sheet silicates. *Journal of Physics C: Solid State Physics*, 6, 1091–1104.
- Martinez-Alonso, S., Rustad, J.R., and Goetz, A.F.H. (2002) Ab initio quantum mechanical modeling of infrared vibrational frequencies of the OH group in dioctahedral phyllosilicates. Part II: Main physical factors governing the OH vibrations. *American Mineralogist*, 87, 1224–1234.
- McKeown, D.A., Bell, M.I., and Etz, E.S. (1999a) Vibrational analysis of the dioctahedral mica: $2M_1$ muscovite. *American Mineralogist*, 84, 1041–1048.
- (1999b) Raman spectra and vibrational analysis of the trioctahedral mica phlogopite. *American Mineralogist*, 84, 970–976.
- Meade, C., Hemley, R.J., and Mao, H.K. (1993) High-pressure X-ray diffraction of SiO_2 glass. *Physical Review Letters*, 69, 1387–1390.
- Mookherjee, M. and Redfern, S.A.T. (2002) A high-temperature Fourier transform infrared study of the interlayer and Si-O-stretching region in phengite- $2M_1$. *Clay Minerals*, 37, 323–326.
- Ortega-Castro, J., Hernandez-Haro, N., Timon, V., Sainz-Diaz, C.I., and Hernandez-Laguna, A. (2010) High-pressure behavior of $2M_1$ muscovite. *American Mineralogist*, 95, 249–259.
- Parise, J.B., Loveday, J.S., Nelves, R.J., and Kagi, H. (1999) Hydrogen repulsion “transition” in $Co(OD)_2$ at high pressure? *Physical Review Letters*, 83, 328–331.
- Parry, S.A., Pawley, A.R., Jones, R.L., and Clark, S.M. (2007) An infrared spectroscopic study of the OH stretching frequencies of talc and 10-Å phase to 10 GPa. *American Mineralogist*, 92, 525–531.
- Pavese, A., Levy, D., Curetti, N., Diella, V., Fumagalli, P., and Sani, A. (2003) Equation of state and compressibility of phlogopite by in-situ high-pressure X-ray powder diffraction experiments. *European Journal of Mineralogy*, 15, 455–463.
- Poli, S. and Schmidt, M.W. (2002) Petrology of subducted slabs. *Annual Reviews of Earth and Planetary Sciences*, 30, 207–235.
- Raugei, S., Silvestrelli, P.L., and Parrinello, M. (1999) Pressure-induced frustra-

- tion and disorder in $\text{Mg}(\text{OH})_2$ and $\text{Ca}(\text{OH})_2$. *Physical Review Letters*, 83, 2222–2225.
- Redhammer, G.J., Beran, A., Schneider, J., Amthauer, G., and Lottermoser, W. (2000) Spectroscopic and structural properties of synthetic micas on the annite-siderophyllite binary: Synthesis, crystal structure refinement, Mössbauer, and infrared spectroscopy. *American Mineralogist*, 85, 449–465.
- Reguir, E.P., Chakhmouradian, A.R., Halden, N.M., Malkovets, V.G., and Yang, P. (2009) Major- and trace-element compositional variation of phlogopite from kimberlites and carbonatites as a petrogenetic indicator. *Lithos*, 112, 374–384.
- Robert, J.L. and Kodama, H. (1988) Generalization of the correlations between hydroxyl-stretching wavenumbers and composition of micas in the system $\text{K}_2\text{O}-\text{MgO}-\text{Al}_2\text{O}_3-\text{SiO}_2-\text{H}_2\text{O}$: A single model for trioctahedral and dioctahedral micas. *American Journal of Science*, 288A, 196–212.
- Rothbauer, R. (1971) Untersuchung eines $2M_1$ -muscovits mit neutronenstrahlen. *Neues Jahrbuch für Mineralogie Monatshefte*, 143–154.
- Rouxhet, P.G. (1970) Hydroxyl stretching bands in micas: A quantitative interpretation. *Clay Minerals*, 8, 375–388.
- Samson, S.D., Nagy, K.L., and Cotton, W.B. III (2005) Transient and quasi-steady-state dissolution of biotite at 22–25°C in high pH, sodium, nitrate and aluminate solutions. *Geochimica et Cosmochimica Acta*, 69, 399–413.
- Schmidt, M.W., Vielzeuf, D., and Auzanneau, E. (2004) Melting and dissolution of subducting crust at high pressures: the key role of white mica. *Earth and Planetary Science Letters*, 228, 65–84.
- Schroeder, P.A. (1990) Far-infrared, X-ray powder diffraction, and chemical investigation of potassium micas. *American Mineralogist*, 75, 983–991.
- Scott, H.P., Liu, Z., Hemley, R.J., and Williams, Q. (2007) High-pressure infrared spectra of talc and lawsonite. *American Mineralogist*, 92, 814–820.
- Sekine, T., Rubin, A.M., and Ahrens, T.J. (1991) Shock wave equation of state of muscovite. *Journal of Geophysical Research*, 96, 19675–19680.
- Serratos, J.M., and Bradley, W.F. (1958) Determination of the orientation of OH bond axes in layer silicates by infrared absorption. *Journal of Physical Chemistry*, 62, 1164–1167.
- Stockhert, B., Wachmann, M., Kuster, M., and Bimmermann, S. (1999) Low effective viscosity during high pressure metamorphism due to dissolution precipitation creep: the record of HP-LT metamorphic carbonates and siliciclastic rocks from Crete. *Tectonophysics*, 303, 299–319.
- Sudo, A. and Tatsumi, Y. (1990) Phlogopite and K-amphibole in the upper mantle: Implications for magma genesis in subduction zones. *Geophysical Research Letters*, 17, 29–32.
- Tateyama, H., Shimoda, S., and Sudo, T. (1977) Estimation of K-O distance and tetrahedral rotation angle of K-micas from far-infrared absorption spectral data. *American Mineralogist*, 62, 534–549.
- Thomsen, T.B. and Schmidt, M.W. (2008) The biotite to phengite reaction and mica-dominated melting in fluid carbonate-saturated pelites at high pressures. *Journal of Petrology*, 49, 1889–1914.
- Vaughan, M.T. and Guggenheim, S. (1986) Elasticity of muscovite and its relationship to crystal structure. *Journal of Geophysical Research*, 91, 4657–4664.
- Vedder, W. (1964) Correlations between infrared spectrum and chemical composition of mica. *American Mineralogist*, 49, 736–768.
- Vedder, W. and McDonald, R.S. (1963) Vibrations of the OH ions in muscovite. *Journal of Chemical Physics*, 38, 1583–1590.
- Velde, B. (1978) Infrared spectra of synthetic micas in the series muscovite-MgAl celadonite. *American Mineralogist*, 63, 343–349.
- (1983) Infrared OH-stretch bands in potassic micas, talcs and saponites; Influence of electronic configuration and site of charge compensation. *American Mineralogist*, 68, 1169–1173.
- Velde, B. and Couty, R. (1985) Far-infrared spectra of hydrous layer silicates. *Physics and Chemistry of Minerals*, 12, 347–352.
- Williams, Q. (1998) High pressure infrared spectra of feldspars: Constraints on compressional behavior, amorphization and diaplectic glass formation. In M.H. Manghni and T. Yagi, Eds., *Properties of Earth and Planetary Materials at High Pressures and Temperatures*, p. 531–543. American Geophysical Union Press, Washington, D.C.
- (2007) Water, the solid Earth and the atmosphere: The genesis and effects of a wet surface on a mostly dry planet. In D.J. Stevenson, Ed., *Treatise on Geophysics: Evolution of the Earth*, 9, p. 121–143. Elsevier, New York.
- Williams, Q. and Guenther, L. (1996) Pressure-induced changes in the bonding and orientation of hydrogen in FeOOH -goethite. *Solid State Communications*, 100, 105–109.
- Williams, Q. and Hemley, R.J. (2001) Hydrogen in the deep Earth. *Annual Reviews of Earth and Planetary Sciences*, 29, 365–418.
- Williams, Q. and Jeanloz, R. (1989) Static amorphization of anorthite at 300 K and comparison with diaplectic glass. *Nature*, 338, 413–415.
- Williams, Q. and Knittle, E. (1996) Infrared and Raman spectra of fluorapatite at high pressures: Compression-induced changes in phosphate site and Davydov splittings. *Journal of Physics and Chemistry of Solids*, 57, 417–422.
- Williams, Q., Knittle, E., Reichlin, R., Martin, S. and Jeanloz, R. (1990) Structural and electronic properties of Fe_2SiO_5 -fayalite at ultrahigh pressures: Amorphization and gap closure. *Journal of Geophysical Research*, 95, 21549–21563.
- Williams, Q., Kruger, M.B., Hemley, R.J., and Jeanloz, R. (1993) High-pressure infrared spectra of α -quartz, coesite, stishovite and amorphous silica. *Journal of Geophysical Research*, 98, 22157–22170.
- Zhang, M., Redfern, S.A.T., Salje, E.K.H., Carpenter, M.A., and Hayward, C.L. (2010) Thermal behavior of vibrational phonons and hydroxyls of muscovite in dehydroxylation: In situ high-temperature infrared spectroscopic investigations. *American Mineralogist*, 95, 1444–1457.

MANUSCRIPT RECEIVED MARCH 2, 2011

MANUSCRIPT ACCEPTED SEPTEMBER 23, 2011

MANUSCRIPT HANDLED BY GRANT HENDERSON